

Bose-Einstein Condensate Dark Matter Halos confronted with galactic rotation curves

M. Dwornik, Z. Keresztes, E. Kun and L. Á. Gergely
Institute of Physics, University of Szeged, Dóm Tér 9,
Szeged 6720, Hungary

Abstract. We present a comparative confrontation of both the Bose-Einstein Condensate (BEC) and the Navarro-Frenk-White (NFW) dark halo models with galactic rotation curves. We conclude that the BEC model fits better the dwarf galaxy dark matter distribution, but suffers from sharp cut-off in larger galaxies, where the NFW model performs better. In more detail, we employ 6 High Surface Brightness (HSB), 6 Low Surface Brightness (LSB) and 7 dwarf galaxies with rotation curves falling into two classes, based on their shapes. In the first class the rotational velocities increase with radius over the whole observed range, the BEC and NFW models giving comparable fits for both HSB and LSB galaxies, while significantly improving over the NFW fit for dwarf galaxies. This improvement is due to the central density cusp avoidance property of the BEC model. The rotational velocity of HSB and LSB galaxies falling into the second class exhibit long flat plateaus, resulting in a better fit of the NFW model for HSB galaxies, and comparable fits for LSB galaxies. The weaker performance of the BEC model for the HSB type II galaxies is due to the BEC density profiles dropping rapidly to zero outside a nearly constant density core.

1. Introduction

The visible part of most galaxies is embedded in a dark matter (DM) halo of yet unknown composition, observable only through its gravitational interaction with the baryonic matter. Assuming the standard Λ CDM cosmological model, the Planck satellite measurements of the cosmic microwave background anisotropy power spectrum support 4.9% baryonic matter, 26.8% DM and 68.3% dark energy in the Universe [1]; [2].

Investigation of mass distribution of spiral galaxies is an essential tool in the research of DM. Beside the stellar disk and central bulge, most of the galaxies harbour a spherically symmetric, massive DM halo, which dominates the dynamics in the outer regions of the stellar disk. Nevertheless there are examples of galaxies which at larger radii are better described by a flattened baryonic mass distribution (global disk model) [3].

Several DM candidates and alternatives have been proposed, the latter assuming Einstein's theory of gravity breaking down on the galactic scale and above ([4]; [5]; [6]; [7]; [8]; [9]; [10]; [11]; [12]). In brane-world and $f(R)$ -gravity models, the galactic rotation curves could be explained without DM ([13]; [14]; [15]; [16]).

It is well known that hot dark matter (HDM) consisting of light ($m \propto eV$) particles cannot reproduce the cosmological structure formation, as they imply that

the superclusters of galaxies are the first structures to form contradicting CMB observations, according to which superclusters would form at the present epoch [17]. Warm dark matter ($m \propto \text{keV}$) models seem to be compatible with the astronomical observations on galactic and also cosmological scales [18]; [19]. Leading candidates for warm dark matter are the right handed neutrinos, which in contrast with their left handed counterparts do not participate in the weak interaction. The decay of these sterile neutrinos produces high amount of X-rays, which can boost the star formation rate leading to an earlier reionization [20]. The existence of sterile neutrinos was however severely constrained by recent IceCube Neutrino Observatory experiments [21]. Cold dark matter (CDM) also shows remarkably good agreement with observations over kpc scales ([22]; [23]). Particular CDM candidates, like neutralinos (which is stable and can be produced thermally in the early Universe) and other weakly interacting massive particles (WIMPs) originating in supersymmetric extensions of the Standard Model were severely constrained by recent LHC results, rendering them into the range $200\text{GeV} \lesssim m_n \lesssim 500\text{GeV}$ [24]. In a Higgs-portal DM scenario the Higgs boson acts as the mediator particle between DM and Standard Model particles, and it can decay to a pair of DM particles. Very recent constraints established by the ATLAS Collaboration on DM-nucleon scattering cross section impose upper limits of approximately 60 GeV for each of the scalar, fermion and vector DM candidates (see Fig. 4 of Ref. [25]), within the framework of this scenario. While massive compact halo objects (MACHOs) of masses less than 10 solar masses (like white dwarfs, neutron stars, brown dwarfs and unassociated planets, primordial black holes in the astrophysical mass range) were disruled either by Big Bang Nucleosynthesis constraints or microlensing experiments as dominant DM candidates, primordial black holes with intermediate mass could still be viable candidates [26], [27].

Large N-body simulations (e.g. [28]) performed in the framework of the Λ CDM-model (Λ being the cosmological constant) were compatible with CDM halos with central density cusps [29]. They are modeled by the Navarro-Frenk-White (NFW) DM density profile $\rho_{NFW}(r) = \rho_s/(r/r_s)(1 + r/r_s)^2$, where r_s is a scale radius and ρ_s is a characteristic density. Some observations support such a steep cuspy density profile [30], [31], nevertheless certain high-resolution rotation curves instead indicate that the distribution of DM in the centres of DM dominated dwarf and Low Surface Brightness (LSB) galaxies is much shallower, exhibiting a core with nearly constant density [32]. In turn, the baryonic matter distribution may also affect the DM density profile. As shown in Ref. [33] a dark matter core within an isolated, initially cuspy dark matter halo may form due to strong supernova feedback. By contrast, adiabatic contraction of baryonic gas tends to produce even cuspiest dark matter halos [34].

The surface number-density profiles of satellites decline with the projected distance as a power law with the slope $(-2) \div (-1.5)$, while the line-of-sight velocity dispersions decline gradually [35]. These observations support the NFW model on scales of $50 \div 500$ kpc.

In a cosmological setup various scalar field DM models were also discussed ([36], [41] and references therein). A particular scalar field DM model describes light bosons in a dilute gas. The thermal de Broglie wavelength of the particles is $\lambda_T \propto 1/\sqrt{mT}$, which can be large for light bosons ($m < \text{eV}$) and for low temperature. Below a critical temperature (T_c), the bosons' wave packets, which are the order of λ_T overlap, resulting in correlated particles. Such bosons share the same quantum ground state, behaving as a Bose-Einstein condensate (BEC), characterized by a single macroscopic wave function. It has been proposed that galactic DM halos could be gigantic

BECs [37]. The self gravitating condensate is described by the Gross-Pitaevskii-Poisson equation system in the mean-field approximation [38], [39], [40], [10]. In the Thomas-Fermi approximation, a 2-parameter (mass m and scattering length a) density distribution of the BEC halo is obtained [see Eq. (3) below], which is less concentrated towards the centre as compared to the NFW model, relaxing the cuspy halo problem.

In model [42] where a normal dark matter phase with an equation of state $P = \rho c^2 \sigma_{tr}^2$ condensed into a BEC with self-interaction ($\sigma_{tr} = 0.0017$ being the one-dimensional velocity dispersion and c the speed of light), the stability of the BEC halo depends on the particle mass and scattering length. For a given mass the stability occurs for larger scattering length and for given scattering length the stability appears at smaller mass. For the scattering lengths: $a = 10^3$ fm, $a = 10^{-14}$ fm and $a = 10^{-55}$ fm the mass of the BEC particle arises as $m > 1$ eV, $m > 2 \times 10^{-6}$ eV and $m > 4.57 \times 10^{-20}$ eV, respectively. Galactic size stable halos can form with $m > 10^{-24}$ eV (Fig. 3. in Ref. [43]).

A stable BEC halo can form as a result of gravitational collapse [44]. The model has been tested on kpc scales confronting it with galactic rotation curve observations [10]. It was pointed out by [46] that the effects of BEC DM should be seen in the matter power spectrum if the boson mass is in the range $15 \text{ meV} < m < 35 \text{ meV}$ and $300 \text{ meV} < m < 700 \text{ meV}$ for the scattering lengths $a = 10^6$ fm and $a = 10^{10}$ fm, respectively. In Ref. [45] the authors showed that the observed collisional behaviour of DM in the Abell 520 cluster can also be recovered within the framework of the BEC model. All of the mentioned BEC particle masses are consistent with the limit $m < 1.87$ eV imposed from galaxy observations and N-body simulation [47]. A discrepancy was however pointed out between the best fit density profile parameters derived from the strong lensing and the galactic rotational curves data. As a conclusion the BEC halo should be denser in lens galaxies than in dwarf spheroidals [48].

In this work we critically examine the BEC model as a possible DM candidate against rotation curve data, pointing out both advantages and disadvantages over the NFW model. Previous studies on the compatibility of the BEC model and galactic rotation curves were promising, but relied on a less numerous and less diversified set of galaxies than employed here ([49], [50]). The paper has the following structure. The basic properties of the BEC DM model are reviewed in Section 2. In Section 3 a comparison is made between the theoretical predictions of the BEC model and the observed rotation curve data of three types of galaxies, the High Surface Brightness (HSB), LSB and dwarf galaxies. The conclusions are presented in Section 4.

2. The Bose-Einstein condensate galactic dark matter halo

An ideal, dilute Bose gas at very low temperature forms a Bose-Einstein condensate in which all particles are in the same ground state. In the thermodynamic limit, the critical temperature for the condensation is $T_c = 2\pi\hbar^2 (n/\zeta)^{3/2} / mk_B$ [51]. Here n and m are the number density and the mass of the bosons, respectively, $\zeta = 2.612$ is a constant, while \hbar and k_B denote the reduced Planck and Boltzmann constants, respectively. Atoms can be regarded as quantum-mechanical wave packets of the order of their thermal de Broglie wavelength $\lambda_T = \sqrt{2\pi\hbar^2 / (mk_B T)}$. The condition for the condensation $T < T_c$ can be reformulated as $l < \lambda_T / \zeta^{-1/3}$, where l is the average distance between pairs of bosons, and it occurs when the temperature, hence the momentum of the bosons decreases such that their de Broglie wavelengths

overlap. The thermodynamic limit is only approximately realized, the finite size giving corrections to the critical temperature [52], [53], [54], [55]. A dilute, non-ideal Bose gas also displays BEC, on the other hand, the condensate fraction is smaller than unity at zero temperature and the critical temperature is also modified [56], [57], [58], [59]. Experimentally, BEC (which could be formed by bosonic atoms, but also form fermionic Cooper pairs) has been realized first in ^{87}Rb [60], [61], [62], then in ^{23}Na [63], [64], and in ^7Li [65].

In a dilute gas, only two-particle interactions dominate. The repulsive, two-body interparticle potential is approximated as $V_{self} = \lambda\delta(\mathbf{r} - \mathbf{r}')$, with a self-coupling constant $\lambda = 4\pi\hbar^2 a/m$, where a is the scattering length. Then in the mean-field approximation (in case when we neglect the contribution of the excited states) the BEC is described by the Gross-Pitaevskii equation [38], [39], [40]:

$$i\hbar\frac{\partial}{\partial t}\psi(\mathbf{r}, t) = \left[-\frac{\hbar^2}{2m}\Delta + V_{selfgrav}(\mathbf{r}) + \lambda\rho(\mathbf{r}, t) \right] \psi(\mathbf{r}, t) , \quad (1)$$

where $\psi(\mathbf{r}, t)$ is the wave function of the condensate and Δ is the 3-dimensional Laplacian. The probability density $\rho(\mathbf{r}, t) = |\psi(\mathbf{r}, t)|^2$ is normalized to

$$n_0(t) = \int d\mathbf{r}\rho(\mathbf{r}, t) , \quad (2)$$

where $n_0(t)$ is the number of particles in the ground state and $\rho(\mathbf{r}, t)$ the number density of the condensate. The potential $V_{selfgrav}(\mathbf{r})/m$ is the Newtonian gravitational potential produced by the Bose-Einstein condensate.

Stationary solutions of the Gross-Pitaevskii equation can be found in a simple way by using the Madelung representation of complex wave-functions [66], [67], then deriving the Madelung hydrodynamic equations [66]. Madelung's equations can be interpreted as the continuity and Euler equations of fluid mechanics, with quantum corrections included. However, the quantum correction potential in the generalized Euler equation contributes significantly only close to the boundary of the system [68]. In the Thomas-Fermi approximation the quantum correction potential is neglected compared to the self-interaction term. This approximation becomes more accurate as the particle number increases [69].

Assuming a spherically symmetric distribution of the condensate the following solution was found [68], [10]:

$$\rho_{BEC}(r) = \rho_{BEC}^{(c)} \frac{\sin kr}{kr} , \quad (3)$$

where $\rho_{BEC} = m\rho(r)$ and

$$k = \sqrt{\frac{Gm^3}{\hbar^2 a}} . \quad (4)$$

The central density $\rho_{BEC}^{(c)} \equiv \rho_{BEC}(0)$ is determined from the normalization condition (2) as

$$\rho_{BEC}^{(c)} = \frac{n_0 m k^3}{4\pi^2} . \quad (5)$$

The Thomas-Fermi approximation remains valid for $n_0 \gg 1/ka$ [68].

The BEC galactic DM halo's size is defined by $\rho(R_{BEC}) = 0$, giving $k = \pi/R_{BEC}$, i.e.

$$R_{BEC} = \pi\sqrt{\frac{\hbar^2 a}{Gm^3}} . \quad (6)$$

The mass profile of the BEC halo is then given as

$$\begin{aligned} m_{BEC}(r) &= 4\pi \int_0^r \rho_{BEC}(r) r^2 dr \\ &= \frac{4\pi \rho_{BEC}^{(c)}}{k^2} r \left(\frac{\sin kr}{kr} - \cos kr \right). \end{aligned} \quad (7)$$

The BEC halo contributes to the velocity profile of the particles which are moving on circular orbit as dictated by the Newtonian gravitational force [10]. This can be taken into account by the following equation:

$$v^2(r) = \frac{4\pi G \rho_{BEC}^{(c)}}{k^2} \left(\frac{\sin kr}{kr} - \cos kr \right), \quad (8)$$

which needs to be added to the baryonic contribution respectively.

3. Confronting the model with rotation curve data

The validity of our model was tested by confronting the rotation curve data of a sample of 6 HSB, 6 LSB and 7 dwarf galaxies, with both the NFW DM and the BEC density profiles. For reasons to become obvious during our analysis, we split both the HSB and LSB data sets into two groups (type I. and II.), based on the shapes of the curves. In the first group the rotational velocities increase over the whole observed range, while in the second set the rotation curves exhibit long flat regions.

The commonly used NFW model has the mass density profile

$$\rho_{NFW}(r) = \frac{\rho_s}{(r/r_s)(1+r/r_s)^2}, \quad (9)$$

where ρ_s and r_s are a characteristic density and distance scale, to be determined from the fit.

The mass within a sphere with radius $r = yr_s$ is then given as

$$m_{NFW}(r) = 4\pi \rho_s r_s^3 \left[\ln(1+y) - \frac{y}{1+y} \right] \quad (10)$$

where y is a positive dimensionless radial coordinate.

3.1. HSB galaxies

In this subsection we will follow the method described in [15]. In a HSB galaxy the baryonic component was decomposed into a thin stellar disk and a spherically symmetric bulge. It was assumed that the mass distribution of bulge component follows the de-projected luminosity distribution with a factor known as the mass-to-light ratio. The bulge parameters were estimated from a Sérsic $r^{1/n}$ bulge model, which was obtained by the fitting of the optical I-band galaxy light profiles.

Each galaxy's spheroidal bulge component has a surface brightness profile which is described by a generalized Sérsic function [70]

$$I_b(r) = I_{0,b} \exp \left[- \left(\frac{r}{r_0} \right)^{1/n} \right], \quad (11)$$

wherein $I_{0,b}$ is the central surface brightness of the bulge, r_0 is the characteristic radius of the bulge and the magnitude-radius curve's shape parameter is denoted by n .

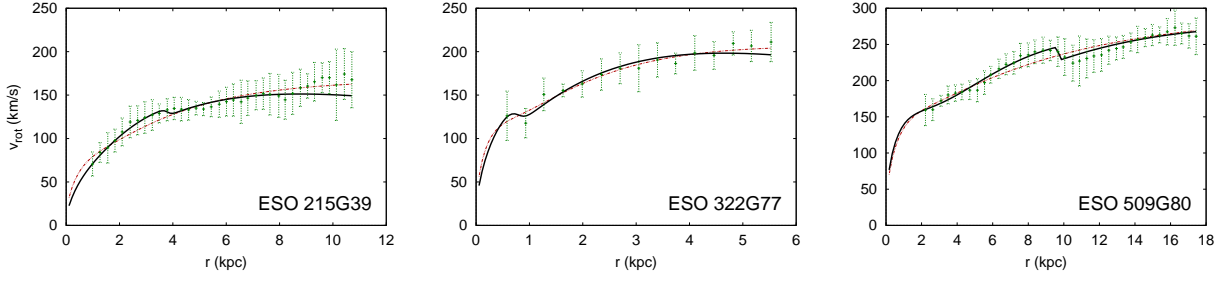


Figure 1. Best fit curves for the HSB I. galaxy sample where the solid black lines hold for the baryonic matter + BEC model, while the dashed red lines refer to the baryonic matter + NFW model.

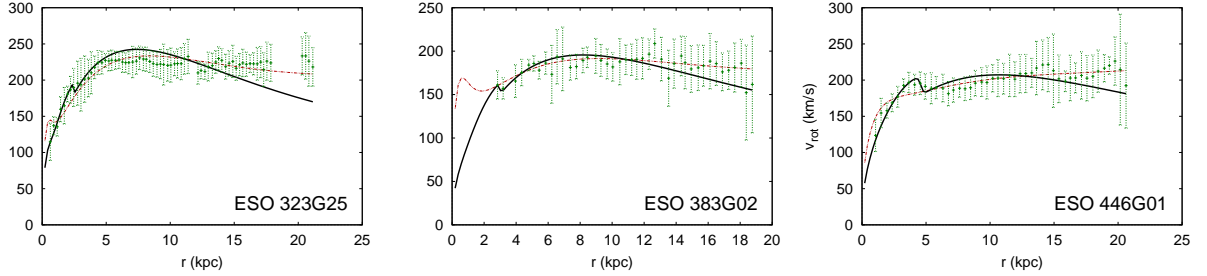


Figure 2. Best fit curves for the HSB II. galaxy sample. The solid black lines hold for the baryonic matter + BEC model, while the dashed red lines for the baryonic matter + NFW model. The BEC model does not describe well the extended flat regions.

Galaxy	D	$I_{0,b}$	n	r_0	r_b	$I_{0,d}^{HSB}$	h^{HSB}
	Mpc	mJy/arcsec ²		kpc	kpc	mJy/arcsec ²	kpc
ESO215G39	61.29	0.1171	0.6609	0.78	2.58	0.0339	4.11
ESO322G77	38.19	0.1949	0.7552	0.33	1.37	0.0744	2.20
ESO509G80	92.86	0.2090	0.7621	1.10	4.69	0.0176	11.03
ESO323G25	59.76	0.1113	0.4626	0.43	0.99	0.0825	3.47
ESO383G02	85.40	0.6479	0.7408	0.42	1.94	0.5118	3.82
ESO446G01	98.34	0.2093	0.8427	1.28	6.33	0.0357	5.25

Table 1. The distances (D) and the photometric parameters of the 6 HSB galaxy sample as determined by the fit with available photometric data [72]. Bulge parameters: the central surface brightness ($I_{0,b}$), the shape parameter (n), the characteristic radius (r_0) and radius of the bulge (r_b). Disk parameters: central surface brightness ($I_{0,d}^{HSB}$) and length scale (h^{HSB}) of the disk.

The mass-to-light ratio for the Sun is $\gamma_{\odot} = 5133 \text{ kg W}^{-1}$. The mass-to-light ratio of the bulge σ will be given in units of γ_{\odot} (solar units). We will also give the mass in units of the solar mass $M_{\odot} = 1.98892 \times 10^{30} \text{ kg}$. We assume that the radial distribution of visible mass follows the radial distribution of light derived from the bulge-disk decomposition. Accordingly the mass of the bulge inside the projected radius r can be derived from the surface brightness observed within this radius:

$$m_b(r) = \sigma \frac{\mathcal{N}(D)}{F_{\odot}} 2\pi \int_0^r I_b(r) r dr,$$

where $F_{\odot}(D)$ is the apparent flux density of the Sun at a distance D Mpc, $F_{\odot}(D) = 2.635 \times 10^{6-0.4f_{\odot}} \text{ mJy}$, with $f_{\odot} = 4.08 + 5 \lg(D/1 \text{ Mpc}) + 25 \text{ mag}$, and

$$\mathcal{N}(D) = 4.4684 \times 10^{-35} D^{-2} \text{ m}^{-2} \text{ arcsec}^2. \quad (12)$$

The rotational velocity related to the bulge

$$v_b^2(r) = \frac{G m_b(r)}{r}, \quad (13)$$

where G is the gravitational constant.

In case of a spiral galaxy, the radial surface brightness profile of the disk, decreases exponentially as a function of the radius [71]

$$I_d(r) = I_{0,d}^{HSB} \exp\left(-\frac{r}{h^{HSB}}\right), \quad (14)$$

where $I_{0,d}^{HSB}$ is the central surface brightness of the disk and h^{HSB} is a characteristic disk length scale. The disk contributes to the circular velocity as follows ([71])

$$v_d^2(x) = \frac{GM_D^{HSB}}{2h^{HSB}} x^2 (I_0 K_0 - I_1 K_1), \quad (15)$$

where $x = r/h^{HSB}$ and I_n and K_n are the modified Bessel functions evaluated at $x/2$, while M_D^{HSB} is the total mass of the disk.

Accordingly in a HSB galaxy the rotational velocity adds up as

$$v_{ig}^2(x) = v_b^2(x) + v_d^2(x) + v_{DM}^2(x). \quad (16)$$

In order to validate the BEC+baryonic model with (HI and H_{α}) compare it with the data of the rotation curve of 6 well-tested galaxies already employed in [15] for testing a brane-world model. The data was obtained from a sample given in [72]. The applied data has to meet the following requirements: i) data has to be as accurate as possible data for each galaxy and ii) bulge has to be spherically symmetric. To validate our model, the NFW+baryonic model is also applied to the same data set. The respective rotation curves are plotted for both models on Figs. 1 and 2. The small humps on both figures are due to the baryonic component. From the available photometric data the best fitting values were derived for the baryonic model parameters $I_{0,b}$, n , r_0 , r_b , $I_{0,d}^{HSB}$, h^{HSB} . By fitting BEC and NFW models to the investigated rotation curve data, the parameters for these models (as well as the corresponding baryonic parameters) were calculated. The parameter values are indicated in Tables 1 and 2.

Both the BEC and NFW DM models give comparable χ_{\min}^2 values (within 1σ confidence level) for HSB I galaxies. In case of galaxies with extended flat regions (HSB II), the NFW DM model fits better the rotation curves, nevertheless BEC model give rotational curves which fall outside the 1σ confidence level.

Galaxy	$\sigma(\text{BEC})$	$M_D^{\text{HSB}}(\text{BEC})$	R_{BEC}	$\rho_{\text{BEC}}^{(c)}$	$\chi_{\text{min}}^2(\text{BEC})$	$\sigma(\text{NFW})$	$M_D^{\text{HSB}}(\text{NFW})$	r_s	ρ_s	$\chi_{\text{min}}^2(\text{NFW})$	1σ
	\odot	$10^{10} M_\odot$	kpc	$10^{-24} kg/m^3$		\odot	$10^{10} M_\odot$	kpc	$10^{-24} kg/m^3$		
ESO215G39	0.3	5.61	3.8	2.0	23.07	0.6	3.84	187	14.7	22.22	34.18
ESO322G77	1.6	5.1	0.8	89.0	9.15	2.5	3.79	709	8	7.69	11.53
ESO509G80	1.4	48.74	9.7	1.2	12.52	0.9	11	22	800	33.48	36.3
ESO323G25	2.5	12.18	2.5	11.8	222.74	6	9.43	436	6	80.55	66.74
ESO383G02	0.13	8.77	3.0	5.7	48.83	1.7	6.32	459	4.2	23.3	47.9
ESO446G01	0.6	12.77	4.6	5.9	86.02	1.4	6.7	786	4.1	43.37	44.74

Table 2. The best fit parameters and the minimum values (χ_{min}^2) of the χ^2 statistics for the HSB I and II galaxies (the first and last three galaxies, respectively). Columns 2-5 give the BEC model parameters (radius R_{BEC} and central density $\rho_{\text{BEC}}^{(c)}$ of the BEC halo) and the corresponding baryonic parameters (mass-to-light ratio $\sigma(\text{BEC})$ of the bulge and total mass of the disk $M_D^{\text{HSB}}(\text{BEC})$). Columns 7-10 give the NFW model parameters (scale radius r_s and characteristic density ρ_s of the halo) and the corresponding baryonic parameters (mass-to-light ratio $\sigma(\text{NFW})$ of the bulge and total mass of the disk $M_D^{\text{HSB}}(\text{NFW})$). The 1σ confidence levels are shown in the last column (these are the same for both models). For HSB I galaxies the two models give similar χ_{min}^2 values (within 1σ confidence level), however in case of HSB II galaxies with extended flat regions, the NFW model fits better the rotation curves. The χ_{min}^2 values in the case of BEC model are outside the 1σ confidence level for HSB II galaxies.

3.2. LSB galaxies

The surface brightness of LSB galaxies is substantially fainter than the brightness of the sky at night. They belong to an early stage class of galaxies [73]. LSB galaxies were found to be metal poor, which indicates a lower star formation rate than what is generally found in HSB galaxies [74]. Wide spectrum of colors can be measured in case of LSB galaxies ranging from red to blue [75] and they are diverse as regards morphologies and other properties. Most of the LSB galaxies that were observed are dwarf galaxies, however there is also a significant number of large spirals among LSB galaxies [76].

According to our model the LSB galaxy is made up of two main components; one being a thin stellar+gas disk and the other one being a CDM component which is assumed to be a BEC. We use the same model for the disk component as in the case of the HSB galaxies. The surface brightness profile can be described by the following equation [71]

$$I_d(r) = I_{0,d}^{\text{LSB}} \exp\left(-\frac{r}{h^{\text{LSB}}}\right),$$

where $I_{0,d}^{\text{LSB}}$ is the central surface brightness and h^{LSB} the disk length scale. The contribution of the disk to the circular velocity can be expressed as

$$v_d^2(r) = \frac{GM_D^{\text{LSB}}}{2h^{\text{LSB}}} q^2 (I_0 K_0 - I_1 K_1), \quad (17)$$

where $q = r/h^{\text{LSB}}$ and M_D^{LSB} is the total mass of the disk while the modified Bessel functions I_n and K_n are evaluated at $q/2$.

Consequently, for an arbitrary projected radius r the rotational velocity can be calculated based on the combined model resulting in the following equation

$$v_{\text{tg}}^2(r) = v_d^2(r) + v_{DM}^2.$$

A preliminary check confirmed that the BEC+baryonic model represents a better fit than the purely BEC model.

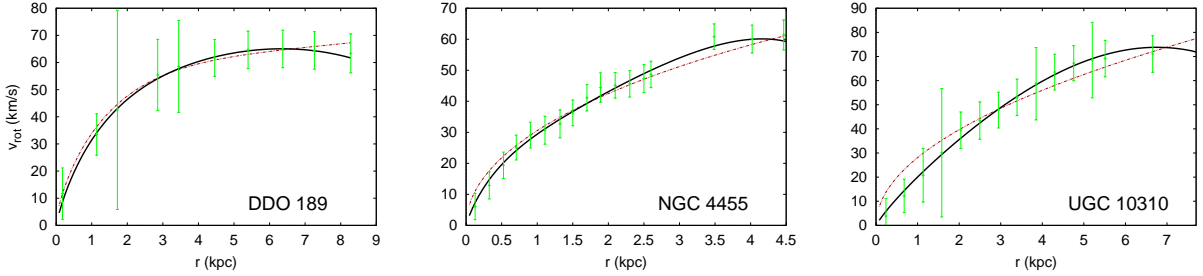


Figure 3. Best fit curves for the LSB I. galaxy sample. The solid black lines indicates the baryonic matter + BEC model, while the dashed red lines indicates the baryonic matter + NFW model.

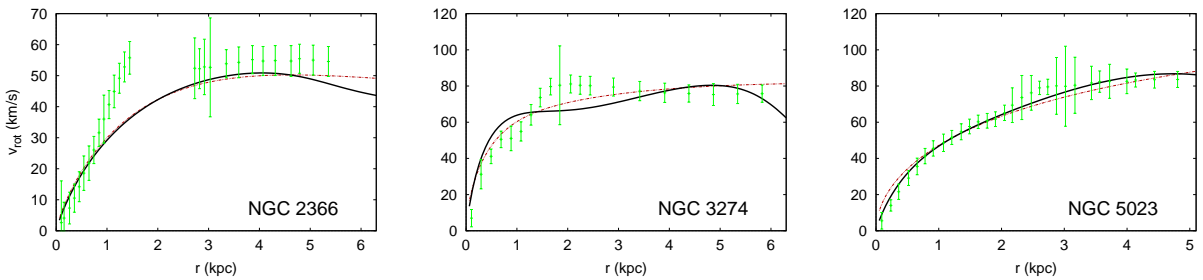


Figure 4. Best fit curves for the LSB II. galaxy sample. The solid black lines refer to the baryonic matter + BEC model, while the dashed red lines to the baryonic matter + NFW model. As for HSB galaxies, the BEC model fails to explain the extended flat regions of the rotation curves.

We confronted the BEC model with 6 LSB galaxies chosen from a larger sample [77]. The applied data were obtained from both HI and $H\alpha$ measurements. From a χ^2 -test the parameters in both the BEC+baryonic and NFW+baryonic models were identified, these are shown in Table 3. The best fit rotation curves are represented on Figs. 3 and 4.

For the LSB I galaxies the BEC DM model gives significantly better fitting velocity curves (all within the 1σ confidence level) compared to the NFW model (which in two cases out of the three gives fits falling outside 1σ). For LSB II galaxies the quality of the fits are comparable, but in both models they are beyond the 1σ confidence level.

3.3. Dwarf galaxies

Approximately 85% of the explored galaxies in the Local Volume [78] are dwarf galaxies. The dwarfs are defined by having an absolute magnitude which is fainter than $M_B \sim -16 \text{ mag}$. On the other hand they are larger than globular clusters [79].

Although little is known about their formation it is generally accepted that dwarfs are formed at the centres of subhalos. Dwarf galaxies can be categorised in five groups

Galaxy	D	h^{LSB}	$M_D^{LSB}(BEC)$	$\rho_{BEC}^{(c)}$	R_{BEC}	$\chi_{\min}^2(BEC)$	$M_D^{LSB}(NFW)$	ρ_s	r_s	$\chi_{\min}^2(NFW)$	1σ
	Mpc	kpc	$10^9 M_{\odot}$	$10^{-21} kg/m^3$	kpc		$10^9 M_{\odot}$	$10^{-23} kg/m^3$	kpc		
DDO 189	12.6	1.9	2.71	0.38	8.3	0.519	2.16	16	70	1.09	7.03
NGC 4455	6.8	2.3	0.231	1.44	5.5	9.29	0.11	25.04	66	5.39	18.11
UGC 10310	15.6	5.2	0.443	0.98	7.8	2.66	0.9	14.9	88	5.76	13.74
NGC 2366	3.4	1.5	2.43	0.22	5.3	110.73	2.5	0.2	1000	116.93	26.72
NGC 5023	4.8	0.8	0.894	2.45	5.6	53.2	0.0449	457	13	143.08	32.05
NGC 3274	6.7	0.5	1.1	1.69	6.4	269.8	0.252	2373	4	148.44	20.27

Table 3. The best fit BEC and NFW parameters of the LSB I and II type galaxies (the first and last three galaxies, respectively). D is taken from [77]. The rest of the parameters are rotation curve fits. For LSB I galaxies the BEC DM model gives significantly better fitting velocity curves (within 1σ confidence level) than the NFW model. However the velocity curves are outside the 1σ confidence level for LSB II galaxies.

according to their optical appearance. The five groups being dwarf ellipticals, dwarf irregulars, dwarf spheroidals, blue compact dwarfs, and dwarf spirals. The dwarfs falling in the last group represent the very small ends of spirals [80]. Dwarf spheroidals are old systems and among the most DM dominated galaxies in the Universe.

The central velocity dispersion of most dwarf galaxies is in the range $6 \div 25$ km/s [81]. In a typical dwarf galaxy, assuming dynamical equilibrium, the mass derived from the observed velocity dispersions is substantially greater than the observed total visible mass. This implies that the mass-to-light ratio is very high compared to other types of galaxies, hence they can greatly contribute to the understanding of DM distribution on small scales. Dwarf galaxies allow for proving or falsifying different alternative gravity theories [82].

We decided to use 7 dwarf galaxies for testing the BEC model. We have selected the sample dwarf galaxies such as to ensure that sufficient high resolution rotation curve data would be available for our study. We fitted both the BEC+baryonic and the NFW+baryonic models, respectively, with similar baryonic components as for the LSB galaxies. As the length scales of the stellar disks were not available for the selected sample, they were calculated by χ^2 minimization, too.

A preliminary check showed that the addition of the BEC dark matter halo to the baryonic model improved (giving lower χ_{\min}^2 values) on the fit in all cases. By contrast, the NFW model was unable to improve on the purely baryonic fit in four out of seven cases. We note that since the data does not contain the error margins, the χ_{\min}^2 values are relatively high (beyond the 1σ confidence level in most cases). The best fit BEC and NFW parameters are shown in Table 4 and the corresponding rotation curves are represented on Fig. 5. The inclusion of the BEC DM model gives significantly (in some cases one order of magnitude in the value of χ^2) better fits compared to the case of NFW model. This is due to the cusp avoidance in the central density profile of the BEC model and the fact that dwarf galaxies do not exhibit extended flat regions in their rotation curves.

4. Discussions and final remarks

We have performed a χ^2 -test of the BEC and NFW DM models, with the rotation curves of 6 HSB, 6 LSB and 7 dwarf galaxy samples. For improved accuracy we also included realistic baryonic models in every case. For the HSB galaxy sample, both the rotation curve and the surface photometry data were available. Most of the rotation

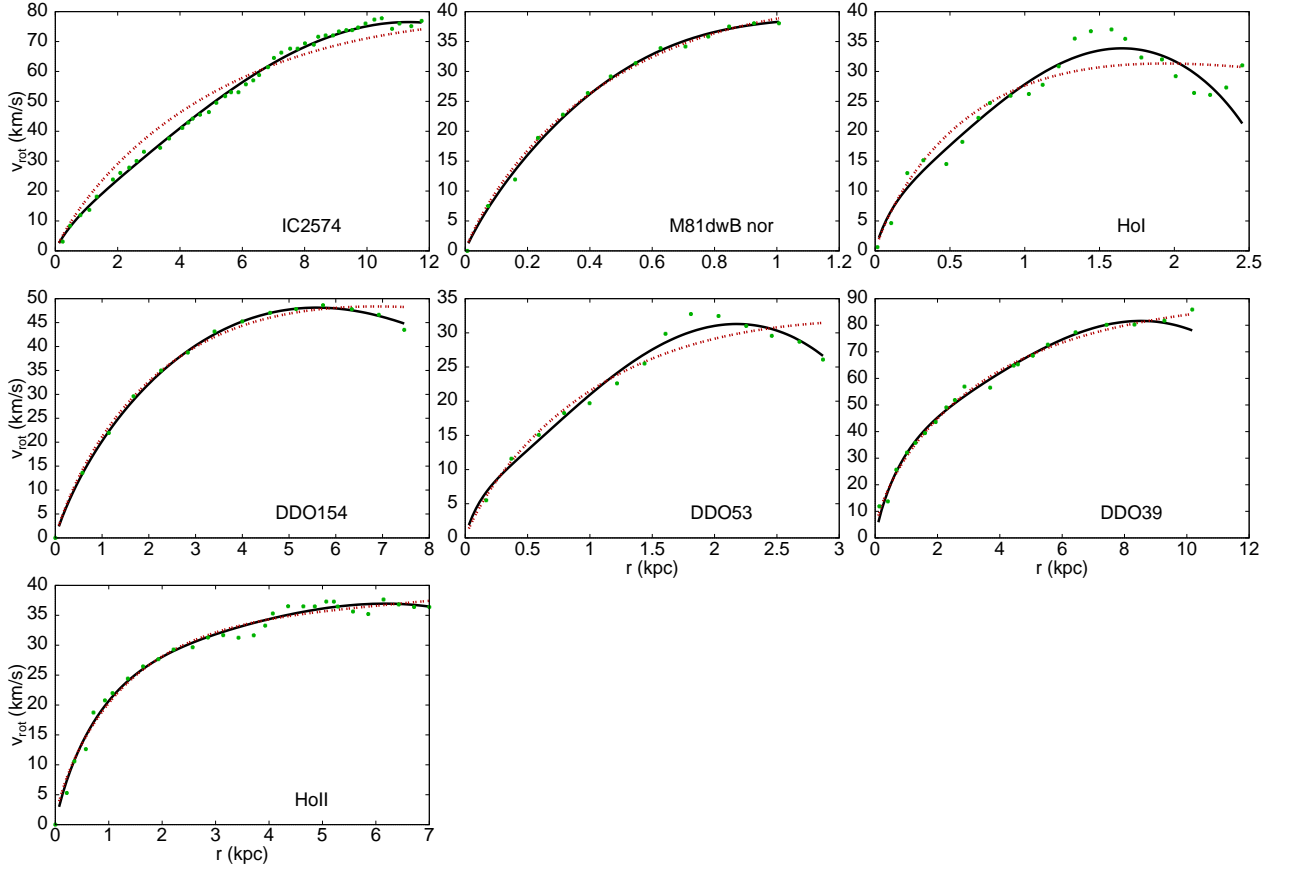


Figure 5. The best fit curves for the dwarf galaxy sample. The BEC+baryonic model (solid black curves) gives a better fit in all cases than the NFW+baryonic model (dashed red lines). In both cases the fit was performed with the same baryonic model.

Galaxy	$h^{dwarf}(BEC)$	$M_D^{dwarf}(BEC)$	$\rho_{BEC}^{(c)}$	R_{BEC}	$\chi_{min}^2(BEC)$	$h^{dwarf}(NFW)$	$M_D^{dwarf}(NFW)$	ρ_s	r_s	$\chi_{min}^2(NFW)$	1σ
	<i>kpc</i>	$10^9 M_\odot$	10^{-24}kg/m^3	<i>kpc</i>		<i>kpc</i>	$10^9 M_\odot$	10^{-24}kg/m^3	<i>kpc</i>		
IC 2574	1.2	0.1122	0.4	13	68.47	7.9	28.44	0	0	714.73	44.74
HoI	0.2	0.0107	3.6	1.9	95.26	0.9	0.533	0	0	241.30	20.27
HoII	1.2	0.4431	0.2	7.69	33.33	1.7	0.642	4	92	43.86	26.72
DDO 39	1.3	1.1235	0.7	10.01	69.39	4.3	7.21	43	35	69.82	17.02
DDO 53	0.2	0.0061	1.8	2.5	20.05	1.6	0.976	1	24	51.53	10.42
DDO 154	3.1	3.3502	0.2	5.8	1.48	3.2	4.52	0	0	9.40	9.30
M81dwB nor	0.9	1.023	3.7	0.7	6.19	0.7	0.705	0	0	8.4	10.42

Table 4. The best rotation curve data fit BEC+baryonic and NFW+baryonic parameters for the dwarf galaxy sample.

curves were smooth, symmetric and uniform in quality.

The circular velocity of the investigated galaxies was decomposed into its barionic and DM contribution: $v_{model}^2(r) = v_{baryonic}^2 + v_{DM}^2$. For the BEC model the DM contribution to the rotational velocity can be described as Eq. (8). Then the rotation curves are fitted with the parameters of the baryonic and DM halo models (BEC and NFW) using χ^2 minimization method.

The analysis of the *HSB I galaxies* showed a remarkably good agreement for both DM models with observations. The BEC and NFW models show similar fits. However, the rotation curves of the HSB II type galaxies are significantly better described by the NFW model.

It was previously known that for *LSB galaxies and without including the baryonic sector*, the BEC model gave a better fit than the NFW model [49]. We additionally found that including the baryonic component improves on the fit of [49]. Our detailed analysis showed a significantly better performance of the BEC model for LSB type I galaxies, while comparable fits for LSB type II galaxies. These latter fits were however outside the 2σ confidence level.

The unsatisfactory large distance behaviour of the BEC model for both the HSB and LSB galaxies of type II originates in the sharp cutoff of the BEC DM distribution and clearly indicates that it would be desirable to modify the BEC model on larger scale, also to comply with the behaviour of the universal rotation curves (URCs) at larger radii [83].

From the above analysis of HSB and LSB galaxies it is also obvious that (while on large distances the BEC model suffers from problems due to the sharp cutoff) close to the it works overall better than the NFW model. This is also supported by our fit of both the BEC+baryonic and NFW+baryonic DM models with rotation curve data of a sample of 7 dwarf galaxies. Since dwarf galaxies are DM dominated, they allow for the best comparison between the various models. The results can be seen in Fig. 5. We also note that the NFW DM improved over the pure baryonic fit in four cases out of seven, while including the BEC component improved over the fit with the baryonic component in all cases.

The BEC parameters were determined for all cases. The parameters $\rho_{BEC}^{(c)}$, R_{BEC} are given in Tables 2, 3, 4. The averages of the radii R_{DM} of the BEC halos for the HSB, LSB and dwarf galaxies are $\langle R_{BEC}^{HSB} \rangle \approx 4.06\text{kpc}$, $\langle R_{DM}^{LSB} \rangle \approx 6.48\text{kpc}$ and $\langle R_{DM}^{dwarf} \rangle \approx 5.94\text{kpc}$, respectively. The scatter however is large, there are no universal BEC parameters which globally fit all the galaxies, not even at 3σ confidence level. The closer to this goal were the HSB galaxies, where 3 out of 6 had overlapping 3σ domains. Nonetheless the given values of R_{DM} are consistent within the order of magnitude with the halo radii of 59 other galaxies determined from weak lensing [84].

There is a relation among the mass m of the BEC particle, its coherent scattering length a and the radius of the DM halo R_{DM} [10]:

$$m = \left(\frac{\pi^2 \hbar^2 a}{GR_{BEC}^2} \right)^{1/3} \approx 6.73 \times 10^{-2} [a(\text{fm})]^{1/3} [R_{BEC}(\text{kpc})]^{-2/3} \text{ eV}. \quad (18)$$

Assuming the BEC is formed of axions with mass of 10^{-6}eV , the scattering lengths for the three types of galaxies emerge as $a_{HSB} \approx 5.4 \times 10^{-14}\text{fm}$, $a_{LSB} \approx 1.37 \times 10^{-13}\text{fm}$ and $a_{dwarf} \approx 1.15 \times 10^{-13}\text{fm}$. These values are consistent with the results of [84], which are based on a statistical analysis of 61 DM dominated galaxies. The total

energy of the BEC halo is negative with these scattering lengths and particle mass, meaning the halo is stable (see Fig. 3. of [43]).

Acknowledgments

In the earlier stages of this work MD, ZK and LÁG were supported by the European Union and the State of Hungary, co-financed by the European Social Fund in the framework of TÁMOP 4.2.4. A/2-11-/1-2012-0001 ‘National Excellence Program’. LÁG was also supported by the Japan Society for the Promotion of Science.

References

- [1] Ade P A R, Aghanim N, Armitage-Caplan C, et al., *Planck 2013 results. I. Overview of products and scientific results*, 2014 *A&A* **571**, 1
- [2] Francis M, *First Planck results: the Universe is still weird and interesting*, 2013 *Arstechnica*
- [3] Jalocha J, Bratek L, Kutschera M and Skindzier P., *Global disk model for galaxies NGC 1365, NGC 6946, NGC 7793, UGC 6446*, 2010 *MNRAS* **406**, 2805-2816
- [4] Milgrom M, *A Modification of the Newtonian dynamics as a possible alternative to the hidden mass hypothesis*, 1983 *ApJ* **270**, 365
- [5] Sanders R H, *Anti-gravity and galaxy rotation curves*, 1984 *A&A* **136**, L21
- [6] Moffat J W and Sokolov I Y, *Galaxy dynamics predictions in the nonsymmetric gravitational theory*, 1996 *Phys. Lett. B* **378**, 59
- [7] Mannheim P D, *Are galactic rotation curves really flat?*, 1997 *ApJ* **479**, 659
- [8] Roberts M D, *Galactic metrics*, 2004 *Gen. Rel. Grav.* **36**, 2423
- [9] Boehmer C G and Harko T, *On Einstein clusters as galactic dark matter halos*, 2007 *MNRAS* **379**
- [10] Boehmer C G, Harko T, *Can dark matter be a Bose-Einstein condensate?*, 2007 *JCAP* **06**, 025
- [11] Bertolami O, Boehmer C G, Harko T and Lobo F S N, *Extra force in f(R) modified theories of gravity*, 2007 *Phys. Rev. D* **75**, 104016
- [12] Boehmer C G, Harko T, Lobo F S N, *Dark matter as a geometric effect in f(R) gravity*, 2008 *Astropart. Phys.* **29**, 386
- [13] Mak M K and Harko T, *Can the galactic rotation curves be explained in brane world models?*, 2004 *Phys. Rev. D* **70**, 024010
- [14] Rahaman F, Kalam M, DeBenedictis A, Usmani A A and Saibal R, *Galactic rotation curves and brane world models*, 2008 *MNRAS* **389**, 27
- [15] Gergely L Á, Harko T, Dwornik M, Kupi G and Keresztes Z, *Galactic rotation curves in brane world models* 2011 *MNRAS* **415**, 3275
- [16] Stabile A and Capozziello P, 2013 *Phys. Rev. D* **87**, 064002
- [17] Primack J R and Gross M A K, *Current Aspects of Neutrino Physics (Springer, Berlin Heidelberg 2000)*, 2000
- [18] de Vega H J and Sanchez N G, *Warm dark matter in the galaxies: theoretical and observational progresses. Highlights and conclusions of the chalonge meudon workshop 2011*, 2011 *arXiv:1109.3187*
- [19] Wei H, Chen Z and Liu J, *Cosmological Constraints on Variable Warm Dark Matter*, 2013 *Phys. Lett. B* **720**, 271-276
- [20] Biermann P L and Kusenko A, *Relic keV sterile neutrinos and reionization*, 2006 *Phys.Rev.Lett.* **96**, 091301
- [21] IceCube Collaboration: Aartsen M G et al., *Searches for Sterile Neutrinos with the IceCube Detector*, 2016 *Phys.Rev.Lett.* **117**, 071801
- [22] Padmanabhan T, *Cosmological constant: The Weight of the vacuum*, 2003 *Phys. Repts.* **380**, 235
- [23] Peebles P J E and Ratra B, *The Cosmological constant and dark energy*, 2003 *Rev. Mod. Phys.* **75**, 559
- [24] Fowlie A, Kowalska K, Roszkowski L, Sessolo E M and Tsai Y L S, *Dark matter and collider signatures of the MSSM*, 2013 *Phys.Rev. D.* **88**, 055012
- [25] Aad G et al. (ATLAS Collaboration), *Search for Invisible Decays of a Higgs Boson Produced in Association with a Z Boson in ATLAS*, 2014 *Phys. Rev. Lett.* **112**, 201802
- [26] Frampton P H, *Angular Momentum of Dark Matter Black Holes*, arXiv:1608.05009 [gr-qc]

- [27] Sasaki M, Suyama T, Tanaka T, Yokoyama S, *Primordial Black Hole Scenario for the Gravitational-Wave Event GW150914*, 2016 *Phys. Rev. Lett.* **117**, 061101
- [28] Volker Springel, Simon D M White, Adrian Jenkins, Carlos S Frenk, Naoki Yoshida, Liang Gao, Julio Navarro, Robert Thacker, Darren Croton, John Helly, John A Peacock, Shaun Cole, Peter Thomas, Hugh Couchman, August Evrard, Joerg Colberg and Frazer Pearce, *Simulating the joint evolution of quasars, galaxies and their large-scale distribution*, 2005 *Nature* **435**, 629
- [29] Navarro J F, Frenk C S and White S D M, *The Structure of cold dark matter halos*, 1996 *ApJ* **462**, 563
- [30] Valenzuela O, Rhee G, Klypin A, Governato F, Stinson G, Quinn T and Wadsley J , *Is there Evidence for Flat Cores in the Halos of Dwarf Galaxies?: The Case of NGC 3109 and NGC 6822*, 2006 *ApJ* **657**, 773-789
- [31] Jardel J R, Gebhardt K, Fabricius M, Drory N and Williams M J, *Measuring Dark Matter Profiles Non-Parametrically in Dwarf Spheroidals: An Application to Draco*, 2012 *ApJ* **763**
- [32] Burkert A, *Aspects of Dark Matter in Astro-and Particle Physics*, 1997
- [33] Teyssier R, Pontzen A, Dubois Y and Read J, *Cusp-core transformations in dwarf galaxies: observational predictions*, 2012 *MNRAS* **429**, 3068
- [34] Inoue S and Saitoh T R, *Shallowed cusp slope of dark matter in disc galaxy formation through clump clusters*, 2011 *MNRAS* **418**, 2527
- [35] Klypin A and Prada F, 2009 *ApJ* **690**, 1488
- [36] Gergely L Á and Tsujikawa S, *Effective field theory of modified gravity with two scalar fields: dark energy and dark matter*, 2014 *Phys. Rev. D* **89**, 064059
- [37] Sin S J, *Late time cosmological phase transition and galactic halo as Bose liquid*, 1994 *Phys. Rev. D* **50**, 3650
- [38] Gross E P, *Structure of a quantized vortex in boson systems* *Nuovo Cimento*, 1961 **20**, 454
- [39] Gross E P, 1963, *J. Math. Phys.* **4**, 195
- [40] Pitaevskii L P, 1961, *Zh. Eksp. Teor. Fiz.* **40** , 646
- [41] Rodriguez-Montoya I, Magana J, Matos T and Perez-Lorezana A, *Ultra light bosonic dark matter and cosmic microwave background*, 2010 *ApJ* **721**, 1509
- [42] Harko T, *Cosmological dynamics of dark matter Bose-Einstein Condensation*, 2011 *Phys.Rev.D* **83**, 123515
- [43] Souza J C C and Pires M O C, *Discussion on the energy content of the galactic dark matter Bose-Einstein condensate halo in the Thomas-Fermi approximation*, 2014 *JCAP* **03**, 010
- [44] Harko T, *Gravitational collapse of Bose-Einstein condensate dark matter halos*, 2014, [arXiv:1403.3358]
- [45] Lee J W, Lim S and Choi D, *BEC dark matter can explain collisions of galaxy clusters*, 2008 [arXiv:0805.3827v1]
- [46] Velten H and Wamba E, *Power spectrum for the Bose-Einstein condensate dark matter*, 2012 *Phys.Lett. B* **709** 1-5
- [47] Boyanovsky D, de Vega H J and Sanchez N, *Constraints on dark matter particles from theory, galaxy observations and N-body simulations*, 2008 *Phys. Rev. D* **77**, 043518
- [48] Gonzalez-Morales A X, Diez-Tejedor A, Urena-Lopez L A and Valenzuela O, *Hints on halo evolution in SFDM models with galaxy observations* 2012 *Phys. Rev. D* **87** 02130
- [49] Robles V H and Matos T, *Flat Central Density Profile and Constant DM Surface Density in Galaxies from Scalar Field Dark Matter*, 2012 *MNRAS* **422**, 282-289
- [50] Dwornik M, Keresztes Z and Gergely L Á, *Recent Development in Dark Matter Research* 2014 *Nova Science Publishers* p. 195-219
- [51] Pitaevskii L P and Stringari S, *Bose-Einstein Condensation*, 2003 *Oxford University Press Inc., New York*.
- [52] Grossmann S and Holthaus M, 1995 *Phys. Lett. A* **208**, 188
- [53] Ketterle W and van Druten N J, *Two-Step Condensation of the Ideal Bose Gas in Highly Anisotropic Traps*, 1996 *Phys. Rev. A* **54**, 656
- [54] Kristen K and Toms D J, *Bose-Einstein condensation of atomic gases in a general harmonic-oscillator confining potential trap*, 1996 *Phys. Rev A* **54**, 4188
- [55] Haugerud H, Haugset T and Ravndal F, *Bose-Einstein condensation in anisotropic harmonic traps* , 1997 *Phys.Lett. A* **225**, 18
- [56] Giorgini S, Pitaevskii L and Stringari S, *Theory of ultracold atomic Fermi gases*, 1996 *Phys. Rev. A* **54**, R4633
- [57] Glaum K, Pelster A, Kleinert H and Pfau T, *Critical Temperature of Weakly Interacting Dipolar Condensates*, 2007 *Phys. Rev. Lett.* **98**, 080407
- [58] Schütte M and Pelster A, *Critical Temperature of a Bose-Einstein Condensate with 1/r*

- Interactions*, 2008 Proceedings of the 9th International Conference, 23-28, September, 2007, Dresden, Germany, Eds. Janke W. and Pelster A., World Scientific Publishing Co. Pte. Ltd., 2008. ISBN #9789812837271, pp. 417-420
- [59] Dalfovo F, Giorgini S, Pitaevskii L P and Stringari S, *Theory of Bose-Einstein condensation in trapped gases*, 1999 *Rev. Mod. Phys.* **71**, 463
- [60] Anderson M H, Ensher J R, Matthews M R, Wieman C E and Cornell E A, *Observation of Bose-Einstein Condensation in a Dilute Atomic Vapor*, 1995 *Science* **269**, 198
- [61] Han D J, Wynar R H, Courteille Ph. and Heinzen D J, "Bose-Einstein Condensation of Large Numbers of Atoms in a Magnetic Time-Averaged Orbiting Potential Trap, 1998 *Phys. Rev. A* **57**, R4114
- [62] Ernst U, Marte A, Schreck F, Schuster J and Rempe G, *Bose-Einstein Condensation in a Pure Ioffe-Pritchard Field Configuration*, 1998 *Europhys. Lett.* **41**, 1
- [63] Davis K B, Mewes M O, Andrews M R, van Druten N J, Durfee D S, Kurn D M and Ketterle W, *Bose-Einstein Condensation in a Pure Ioffe-Pritchard Field Configuration*, 1995 *Phys. Rev. Lett.* **75**, 3969
- [64] Hau L V, Busch B D, Liu C, Dutton Z, Burns M M and Golovchenko J A, *Near Resonant Spatial Images of Confined Bose-Einstein Condensates in the 4-Dee Magnetic Bottle*, 1998 *Phys. Rev. A* **58**, R54
- [65] Bradley C C, Sackett C A, Tollett J J and Hulet R G, *Evidence of Bose-Einstein condensation in an atomic gas with attractive interactions*, 1995 *Phys. Rev. Lett.* **75**, 1687
- [66] Madelung, E., 1926, *Zeitschrift für Physik* **38**, 322
- [67] Sonogo S, *Interpretation of the hydrodynamical formalism of quantum mechanics*, 1991 *Found. Phys.* **21**, 1135
- [68] Wang X Z, *Cold bose stars: Selfgravitating Bose-Einstein condensates*, 2001 *Phys. Rev D* **64**, 124009
- [69] Lieb E H, Seiringer R and Yngvason Y, *A rigorous derivation of the Gross-Pitaevskii energy functional*, 2000 *Phys. Rev. A* **61**, 043602
- [70] Sérsic J L, 1968, *Atlas de Galaxias Australes*, Cordoba, Argentina, Observatorio Astronomico
- [71] Freeman K C, *On the disks of spiral and SO Galaxies*, 1970 *ApJ* **160**, 811
- [72] Palunas P and Williams T B, *Maximum Disk Mass Models for Spiral Galaxies*, 2000 *ApJ* **120**, 2884
- [73] Impey C and Bothun G, *Low Surface Brightness Galaxies*, 1997 *ARA&A* **35**, 267
- [74] McGaugh S S, *Oxygen abundances in low surface brightness disk galaxies*, 1994 *ApJ* **426**, 135
- [75] O'Neil K, Bothun G D, Schombert J, Cornell M E and Impey C D, *A Wide Field CCD Survey for Low Surface Brightness Galaxies.II.Color Distributions, Stellar Populations, and Missing Baryons*, 1997 *ApJ* **144**, 244
- [76] Beijersbergen M, de Blok W J G and van der Hulst J M, *Surface photometry of bulge dominated low surface brightness galaxies*, 1999 *A&A* **351**, 903
- [77] de Blok W J G and Bosma A, *High-resolution rotation curves of low surface brightness galaxies*, 2002 *A&A* **385**, 816
- [78] Karachentsev I D, Karachentseva V E, Huchtmeier W K and Makarov D I, *A Catalog of Neighboring Galaxies*, 2004 *ApJ* **127**, 2031
- [79] Tammann G A, *Dwarf Galaxies in the Past, in Dwarf Galaxies*, 1994 *ESO Conference and Workshop Proc No. 49* p. 3
- [80] Matthews L D and Gallagher J S, *B and V CCD photometry of southern, extreme late-type spiral galaxies*, 1997 *ApJ* **114**, 5
- [81] Mateo M, *Dwarf galaxies of the Local Group*, 1998 *ARA&A* **36**, 435
- [82] Capozziello S, Cardone V F and Troisi A, *Low surface brightness galaxy rotation curves in the low energy limit of Rn gravity: no need for dark matter?*, 2007 *MNRAS* **375**, 1423
- [83] Persic M, Salucci P and Stel F, *The universal rotation curve of spiral galaxies—I. The dark matter connection*, 1996 *MNRAS* **281**, 27
- [84] Pires M O C and de Souza J C C, *Galactic cold dark matter as a Bose-Einstein condensate of WISPs*, 2012 *JCAP* **11**, 024